DOI: 10.1002/ ((please add manuscript number))
Article type: Full Paper

Low-Voltage Polyelectrolyte-Gated Polymer Field-Effect Transistors Gravure Printed at High Speed on Flexible Plastic Substrates.

*Quentin Thiburce and Alasdair J. Campbell**

Q. Thiburce, Prof. A. J. Campbell
Experimental Solid State Group, Department of Physics, Imperial College London, Blackett Laboratory, South Kensington Campus, London SW7 2AZ, United Kingdom
E-mail: alasdair.campbell@imperial.ac.uk

Keywords: organic electronics, thin-film transistors, polyelectrolyte, electrolyte-gated organic field-effect transistor (EGOFET), gravure printing

We report the fabrication of polymer field effect transistors operating under a bias of |1V| in which the insulator and semiconductor are gravure printed on plastic at the high speed of 0.7 m s^{-1}. Remarkably, the process does not necessitate any surface modification and relies solely on the careful selection and optimization of formulations based on solvent blends. In addition to demonstrating high-throughput fabrication, we fulfill another requirement for organic electronics and achieve low-voltage operation in ambient air by using a polyelectrolyte insulator, poly(4-styrenesulfonic acid) (PSSH). PSSH is a proton conductor that forms electrical double layers at the interfaces with the gate electrode and the semiconductor channel upon application of a small gate voltage (≤ |1 V|). Printed PSSH exhibits a high capacitance of 10 μF cm^{-2}, leading to a printed poly(3-hexylthiophene) (P3HT) hole mobility above 0.1 cm^2 V^{-1} s^{-1} in a bottom-gate, top-contact configuration.

1. Introduction

One of the main advantage of organic materials resides in the fact that they enable the low-cost manufacture of solution-processed integrated circuits on cheap and flexible substrates, such as plastic or paper. In particular, organic thin-film transistors (OTFTs) are promising candidates for use in the backplane and drive circuitry of active-matrix displays,[1] as radio-

frequency identification tags,[2] as well as for a wide range of optical, chemical and biomedical sensing applications.[3-6] In addition to low-cost processing, another requirement is low-voltage operation, in order to enable compatibility with low supply voltage thin-film batteries and low-power consumption for portable devices. Furthermore, when chemical or biomedical sensing is performed in aqueous environments, operating voltages below |1 V| are required because of the small electrochemical window of water.[7] Strategies employed to reduce operating voltages include the use of high permittivity and/or ultra-thin gate dielectrics.[8]

Another approach is to use electrolytes: while they are electronic insulators, they allow the flow of ionic currents, leading to the formation of ultra-thin interfacial electrical double layers (EDLs) yielding very high charge densities upon application of a small potential between two electrodes, allowing low-voltage (≤ |1 V|) transistor operation regardless of the insulator thickness.[9-11] Electrolytes have been successfully employed in OTFTs in the form of liquids, either salts dissolved in a polar solvent[12] or room temperature ionic liquids,[13] and solids when immobilized in a polymer matrix, namely polymer electrolytes[14] and ion gels.[15] Electrolyte-gated OTFTs can operate either as electrolyte-gated organic field-effect transistors (EGOFETs) or organic electrochemical transistors (OECTs), depending on the permeability of the transistor channel to ion penetration, the voltage applied and whether the devices are operated in ambient or inert atmosphere.[11] EGOFETs gated with polyelectrolytes, which are polymers containing ionic groups that dissociate in the presence of air moisture, have also been demonstrated.[16] Solid polyanionic (polycationic) films possess the specificity of having a virtually immobile negatively (positively) charged backbone, thus preventing diffusion of anions (cations) at the interface with a p-type (n-type) semiconductor upon application of a negative (positive) gate voltage, which could otherwise lead to undesired electrochemical doping in EGOFETs.

Previous reports of printed EGOFETs include ion gel-gated devices and circuits fully or partially aerosol-jet printed on Si/SiO_2 and plastic,[17] or prepared using a combination of screen, aerosol-jet and inkjet printing on paper.[18] To the best of our knowledge, only one example of partially printed polyelectrolyte-gated OFETs has been previously reported, in which the authors employed an amphiphilic compatibility layer in order to allow inkjet printing of the semiconducting layer on top of the spin-coated polyelectrolyte.[19] While these are significant achievements, these printing methods are not compatible with high-throughput fabrication. Gravure printing, however, is considered as one of the best candidate for large-area roll-to-roll processing at speeds in the order of 1 m s^{-1} with conventional resolutions between 10 - 100 μm.[20] A highly scaled gravure printing method has also been developed by the Subramanian group, who demonstrated printed features with a resolution below 5 μm.[21] OFETs and organic complimentary circuits with gravure printed polymer dielectrics and p- and n-type polymer semiconductors have been achieved using conventional gravure printing, with operating voltages typically in the range 20 to 80 V.[20,22] Fully printed OFETs and circuits operating within this voltage range have been fabricated via gravure printing, or using a combination of gravure and flexographic or offset printing.[23,24,25] Using a gravure printed photopatterned thin dielectric, operating voltages could be lowered to 10 V.[26] Recently, fully printed OFETs operating below 5 V fabricated using highly scaled (sub-5 μm), high-speed (~ 1 m s^{-1}) gravure printing were reported.[27] Low-voltage OTFTs operating below 2 V, with reverse gravure printed insulator and semiconductor and inkjet printed electrodes were also reported.[28,29] These employed a hygroscopic insulator and their principle of operation is similar to that of an OECT.[30] The state-of-the art gravure printed poly(3-hexylthiophene) (P3HT) field-effect hole mobility reported to date is 0.05 $cm^2 V^{-1} s^{-1}$.[20]

Here, to our knowledge, we report the first EGOFETs with gravure printed polyelectrolyte insulator and semiconductor layers. These are printed at the high speed of 0.7 m s^{-1} on flexible plastic substrates, allowing the rapid preparation of arrays of isolated devices, and easy

integration in a large-area batch process flow to deposit the Au contacts and interconnects. The resultant bottom-gate top-contact EGOFETs have an operating voltage below or equal to |1 V|, the lowest achieved to date for organic transistors with gravure printed layers, while keeping a relatively simple fabrication process. They additionally achieve a very high P3HT hole mobility, exceeding that in other gravure printed transistors.

2. Results and discussion

2.1. Device fabrication

2.1.1. Device geometry

The EGOFET **(Figure 1.a)** has a bottom gate, top contact configuration with thermally evaporated gold gate, source and drain electrodes and is deposited on a flexible polyethylene terephthalate (PET) substrate. The bottom gate configuration was chosen because of the incompatibility between the hydrophobic semiconductor and the water-soluble polyelectrolyte. The top gold source and drain contacts ensured negligible contact resistance. The EGOFET employs two widely used, commercially available polymer layers, in order to allow easy comparison of the gravure printed device performance with previous work. The polyelectrolyte used is poly(4-styrenesulfonic acid) (PSSH) **(Figure 1.b)** and the organic semiconductor is regioregular P3HT **(Figure 1.c)**.

PSSH is a strongly acidic (pH = 1.55 at 25 ºC for 18 wt% in H_2O) sulfonated polyanion with mobile protons as counter ions when exposed to air moisture. Upon application of a small negative potential to the gate electrode – with respect to the grounded source electrode – the protons H^+ diffuse to the PSSH/gate interface to form a thin EDL, leaving charged PSS^- chains at the PSSH/P3HT interface, which, in turn, creates holes in the P3HT in order to maintain interfacial charge neutrality, forming the second EDL.[16] The source and drain electrodes form a channel with a width W = 1000 μm and a length L = 20, 50 or 100 μm, while the gate electrode area was significantly larger than the channel area, in order to ensure a large potential drop at the polyelectrolyte/semiconductor interface. Because the

polyelectrolyte requires a humid environment in order to exhibit sufficient ion mobility, devices were tested in ambient. Consequently, voltages were limited to a maximum of |1 V|, in order to avoid water electrolysis, which could lead to high electrochemical currents and device failure.[7]

2.1.2. Gravure printing

Gravure printing is a fast deposition technique that relies on direct ink transfer from a metal "cliché" onto a flexible substrate. In industrial printers, both the cliché and the impression roll are cylindrical, however, the laboratory scale test printer used in this work employs a flat chromium-plated copper plate as the cliché (the principle of operation is identical) (**Figure 2**). The desired printing features are engraved onto the gravure plate in the form of an array of small ink cells. The shape and density of these ink cells play a key role in the uniformity and thickness of the deposited films. In particular, it was observed that smaller cell densities consistently gave thicker and less uniform films. Hence, the highest density available (250 lines/cm) was chosen for all processed devices.

The printing process starts with the deposition of the ink formulation onto the gravure plate, which is then scraped to fill the engraved ink cells with a metal doctor blade. This step is influenced by the "nip" pressure between the blade and the plate (which also changes the inclination of the blade), as well as their relative speed. The nip pressure was adjusted in order to not observe any ink drag out and kept at a fixed value – in the order of 100 N cm^{-2} – for the duration of the work. The maximum printing speed of the printer (0.7 m s^{-1}) was chosen in order to demonstrate high throughput fabrication. The ink-filled cells are then placed into contact with the substrate, which is mounted on the impression roll, and the ink transfers from the cells to the substrate. With fixed nip pressure and speed parameters, ink rheology is the most important factor to consider for the transfer to be efficient, and careful engineering of the ink viscosity and surface tension is required.[31] The ink droplets deposited from each individual cell subsequently spread and coalesce to form a continuous layer, the solvent

evaporates and the dried ink forms a continuous and homogeneous thin-film. Once again, fine tuning of the ink properties is essential.

2.1.4. Printing of the polyelectrolyte

PSSH is highly soluble in water and soluble in other polar solvents, which is convenient as it allows the formulation of inks without the need to use expensive or toxic solvents. A commercial formulation containing 18 wt% PSSH in water was used as the base for printing the polyelectrolyte. However, the films obtained by printing the unaltered aqueous solution were highly uneven (**Figure 3.a**). This is easily explained by the high contact angle (70º) measured for this formulation on PET (**Figure 4.a**), which results from the high surface tension of water.

Simple strategies to reduce the contact angle include increasing the substrate surface energy by a mild oxygen plasma treatment and/or reducing the solution surface tension by adding a lower surface tension solvent. To enable the gravure printing of a similar water based formulation of PEDOT:PSS on indium tin oxide coated plastic substrates, both approaches were previously used.[31] In order to avoid increasing the complexity of the fabrication process, the second approach was favored and isopropanol was added in various concentrations. At 20 vol% added isopropanol, a large improvement in film homogeneity is observed (**Figure 3.b**). No major changes were observed between 20 and 40 vol% added isopropanol, but the films got visually smoother with 50 vol% isopropanol (**Figure 3.c**). The high film uniformity is also accompanied by the absence of any obvious coffee stain effect. The initial increase in film quality is explained by the two-fold decrease (35º) of the contact angle with 20 vol% isopropanol, which is further decreased to virtually 0º ("perfect" wetting) with 33 vol% isopropanol and above. The addition of a lower surface tension solvent also improves film formation by creating an inward Marangoni flow that counterbalances the outward convective flow which occurs during solvent drying.[31]

In order to gain more insight as to why the film quality seemed to further improve at 50 vol% added isopropanol, the viscosity of the various formulations was measured (**Figure 4.b**). This showed that after an initial increase of the viscosity from 19 mPa s^{-1} with no added isopropanol to 33 mPa s^{-1} at 33 vol% isopropanol, it decreases past this maximum to reach 24 mPa s^{-1} at 50 vol% isopropanol. This non-monotonic dependence of the viscosity with increasing isopropanol concentration has been reported for various water-alcohol mixtures and is attributed to the formation of micelles within the liquid.[32] These micelles result from the attraction of polar alcohol groups to water molecules, leaving the hydrophobic carbon backbones to interact strongly with each other. These interactions lead to mixture viscosities that are higher than the viscosities of both components in their pure state, with a peak in viscosity at about 30% mole fraction of alcohol.[32] The results in Fig 4.b are qualitatively similar, although the presence of the PSSH chains has increased the overall viscosity by a factor of 20 compared to the pure water-alcohol mixtures.

These observations suggest that the lowering of the viscosity of the formulation leads to a general improvement of the film-forming capabilities of the ink. This is in agreement with what was previously reported for gravure printed P3HT, where an increase of viscosity by using a higher solid loading of the ink lead to a 6-fold increase in surface roughness.[20] The surface roughness of the printed PSSH films using the formulation with 50 vol% added isopropanol was indeed very low, with a root mean square roughness $R_{RMS} \approx 1$ nm, as estimated by atomic force microscopy (AFM) (**Figure 3.e**). One drawback, however, of using inks with lower viscosity and surface tension, is that it leads to a decrease in printed feature resolution as a result of spreading. No smaller than 100 μm-wide lines with a separation of 100 μm could be resolved using the 50 vol% isopropanol formulation (**Figure S1**). We note that the printer used in this work has no mechanism for precise alignment of subsequent printed layers, leading to a poor registration accuracy of several hundred microns. The printed features for the devices in this work were therefore kept large compared to the channel area,

so the feature resolution of this formulation on this scale was not an issue. For applications where a higher registration accuracy is needed and a more precise alignment is required (eg. conducting polymer source and drain contacts), a trade-off would have to be found in terms of viscosity and film quality. Higher values lead to a better printing resolution, but at the expense of surface roughness and layer homogeneity which could lead to changes in the electrical properties.

Finally, in order to later realize bottom-gate transistors, it is required that PSSH prints equally well on the PET substrate and the gold gate. Fortunately, the printed PSSH films were seemingly unaffected by the presence of the electrode. No dewetting around the step formed by the edge of the gold pad was observed (**Figure 3.d**), as well as no detectable increase in surface roughness.

2.1.4. Printing of the semiconductor

In order to print the semiconductor on top of PSSH, 10 mg mL^{-1} formulations of P3HT in various solvents were prepared. Both chlorinated solvents – chloroform (bp 61 ºC), chlorobenzene (bp 132 ºC) and 1,2-dichlorobenzene (o-DCB) (bp 178 ºC) – and non-chlorinated solvents – tetrahydrofuran (bp 65 ºC), toluene (bp 110 ºC), xylene (bp 140 ºC), indan (bp 176 ºC) and 1,2,3,4-tetrahydronaphthalene (tetralin) (bp 207 ºC) – were tested. These solvents were chosen for test printing formulations as they cover a wide range of boiling points, have been previously shown to dissolve P3HT,[33] and have been used to gravure-print it.[20, 28] A relatively high molecular weight P3HT (M_w = 67,000) was used, as it has been shown to increase charge mobility.[34] However, this leads to a limited solubility at room temperature, especially in non-chlorinated solvents. The solutions were therefore heated to 60 ºC to increase the solubility. The solutions were observed to reversibly form a gel when cooled down to room temperature. The film-forming capabilities of these formulations were mediocre, showing poor coverage and highly non-uniform layers (**Figure S2**). The worst results were obtained with o-DCB (**Figure 5.a**), while tetralin exhibited a somewhat better

coverage than the other formulations (**Figure 5.b**). Contact angle measurements were inconclusive to explain this behavior as low values (< 10º) were measured, which is most likely a result of the high surface energy of the polar polyelectrolyte. Furthermore, considering only the two highest boiling point solvents, it is expected that the polar surface would have a better affinity with the slightly polar o-DCB than with the non-polar tetralin. The explanation might instead reside in the solubility of P3HT in these two solvents: once a film of the P3HT formulation in tetralin has been deposited on the substrate, it is expected to quickly reach room temperature, leading to the gelification of the film. The subsequent increase in viscosity would effectively block any fluid motion that could result in dewetting of the film. On the other hand, such a phenomenon would not occur with the o-DCB formulation, owing to the high solubility of P3HT in this chlorinated solvent. The slow evaporation rate of o-DCB would then allow a significant time for the dewetting processes to occur within the drying film.

Using the tetralin formulation as the starting point, a similar approach to the one used to print PSSH was adopted and cyclohexane, a lower boiling point, lower surface energy solvent used in a previous work,[31] was blended with tetralin in order to improve the quality of the printed layer. Hence, 10 mg mL^{-1} formulations of P3HT in tetralin and cyclohexane blended in various volume ratio were printed. Excellent coverage and uniformity were obtained for a 1:1 tetralin/cyclohexane volume ratio (**Figure 5.c**). As for PSSH, the improvement in film quality is attributed to the improved wetting resulting from the addition of cyclohexane, as well as the inward Marangoni flow arising from the different evaporation rates of the two solvents in the mixture counterbalancing the outward convective flow. This confirms that using solvent blends is a powerful method for depositing good quality gravure printed thin-films, freeing from the need to use any surface treatment, additives or adhesion layer.

We do note that because a very low solid content was used for the P3HT ink, the resulting printed layers suffer from large edge spreading and relatively poor patterning definition

(**Figure S3**). Once again, the resolution could be easily enhanced by increasing the solid content of the ink – and therefore its viscosity. This would however produce thicker layers, which could in turn increase bulk leakage currents within the semiconductor layer, as well as increasing the contact resistance in the transistor geometry used in this work.

2.2. Device characterization

2.2.1. Polyelectrolyte capacitance

Capacitors employing printed PSSH sandwiched between two gold electrodes were fabricated and their performance was evaluated using impedance spectroscopy. From the measured values of the real part *Z'* and imaginary part *Z''* of the electrical impedance as a function of the frequency *f*, the effective capacitance per unit area $C = 1/(2\pi fZ''A)$, where A is the electrode area, and the phase angle $\theta = \arctan(Z''/Z')$ were computed (**Figure 6**).

The frequency dependence of the phase angle is similar to that previously reported for the same material.[35] It is close to -80º for low frequencies below 10 Hz, as well as for higher frequencies between 10 and 100 kHz, indicating capacitive behavior, while it reaches a local maximum of -65º between these two domains, suggesting a somewhat more resistive component. Above 100 kHz, it quickly rises to reach -20º at 1 MHz, also indicative of a transition towards a resistive behavior. According to previous models,[35] the behavior at the highest frequencies reveals non-ideal contacts, the high frequency capacitance is attributed to dipolar relaxation, the resistance manifesting itself at intermediate frequencies relates to ionic relaxation (proton oscillating around the polymer chains) and the low frequency capacitance corresponds to the formation of the electrical double layers. The associated double layer capacitance per unit area C_i has a high value of 10 μF cm^{-2}.

2.2.2. Transistor characteristics

The electrical performance of the gravure printed EGOFETs were evaluated using the common source configuration (in which the source electrode is grounded) and measuring the output characteristics I_D-V_D at a fixed V_G value between 0 and -1 V (**Figure 7.a**), as well as

the transfer characteristics I_D-V_G with V_D = -1 V (**Figure 7.b**). Thanks to the high value of the double layer capacitance, clear transistor operation is observed even within these small voltage windows, with high measured on current values (>10 μA at $V_D = V_G$ = -1 V) despite the low voltages used.

However, the EGOFETs suffer from a low on/off ratio (~ 60), which is largely due to the very high value of the gate current in the off state (0.5 μA at V_G = 1 V and V_D = -1 V) (Figure 7.b), indicative of large leakage currents between the source/drain contacts and the gate electrode, through the polyelectrolyte. Drain-to-source off-currents within the bulk of the semiconductor film are also likely, owing to the low ambient stability of P3HT, and could not be avoided as the polyelectrolyte requires air moisture to exhibit ionic motion.

To complete the electrical characterization of the devices, the square-root of $|I_D|$ was plotted against V_G to extract the hole mobility $\mu = (2L/WC)(\partial(|I_D|^{0.5})/\partial V_G)^2$ and the threshold voltage V_T by extrapolating the x-axis intercept with the linear part of the curve. Averaging over 10 devices yielded $\mu = 0.16 \pm 0.03$ cm^2 V^{-1} s^{-1} and $V_T = 0.01 \pm 0.05$ V. The threshold voltage is very small and this mobility value is very high for printed P3HT devices operated in air. It is likely due to the extensive filling of trap states within the semiconductor thanks to the very high charge densities resulting from the high double layer capacitance.[36]

Finally, EGOFETs spin-coated on PET substrates were fabricated for comparison. The devices had the same architecture, with a channel width W and length L of 1000 μm and 50 μm, respectively. In order to obtain comparable film thicknesses, PSSH was spin-coated at 4000 rpm from a 9 wt% solution, yielding a thickness of ~ 180 nm and P3HT was spin-coated at 4000 rpm from a 3 mg mL^{-1} solution in the same solvent blend as for gravure-printed devices, which gave a film thickness of ~ 10 nm. The spin-coated devices actually showed poorer performance than their gravure printed counterparts (**Figure S4**), with a lower on current (< 5 μA at $V_D = V_G$ = -1 V), an on/off ratio below 10, a mobility of ~ 0.005 cm^2 V^{-1} s^{-1}

and a threshold voltage of – 0.06 V. AFM measurements were performed in order to try and explain these differences, but the surface morphology of both PSSH and P3HT films prepared by each deposition method were very similar. We believe these electrical performance disparities may instead result from different molecular ordering at the buried PSSH/P3HT interface, arising from the vastly different dynamics of film formation of each deposition method. In particular, gravure printing is a slow drying process, especially when high boiling point solvents such as tetralin are employed, whilst spin-coating leads to a much faster evaporation rate and solidification of the film. In addition, the fact that the polymer layers are not patterned in spin-coated devices could potentially lead to poorer electrical performance such as the distribution of the EDL across a much larger polyelectrolyte/semiconductor surface area. Despite these observations, the results obtained with spin-coated devices do assess the viability of gravure printing as compared to conventional laboratory fabrication methods and confirms that the shortcomings of the EGOFETs reported here can be mostly ascribed to the choice of materials rather than on the printing process itself.

3. Conclusion

In conclusion, we demonstrated the fabrication of EGOFETs on flexible plastic substrates using a very high throughput method, gravure printing, to deposit the polymeric layers at the speed of 0.7 m s^{-1}. No surface modification steps were needed thanks to the optimization of the surface tension of the inks by careful selection of solvent blends. Owing to the high double layer capacitance of the printed polyelectrolyte, the devices exhibited a high hole mobility, a small threshold voltage, high on currents and low voltage transistor operation. However, the transistors did suffer from high off currents, leading to small on/off ratios. This could be resolved by using a more ambient-stable organic semiconductor or another solid electrolyte material such as a poly(ionic liquid) or ion gel, which do not necessitate air moisture to exhibit high ionic motion, thus allowing operation in an inert atmosphere and device encapsulation.

4. Experimental Section

Materials: P3HT (M_w = 67,000 and regioregularity > 95%) was obtained from BASF. PSSH (M_w = 75,000, 18 wt% in H_2O) and solvents were purchased from Sigma Aldrich. The plastic substrates used were 125 mm-thick Melinex ST506 PET foil manufactured by DuPont Teijin.

EGOFET fabrication: The substrates were first rinsed in acetone and isopropanol. The gate electrodes were then deposited by thermally evaporating 50 nm-thick gold pads through a shadow mask. The polymer layers were subsequently either spin-coated at 4000 rpm or printed using a Labratester 1 laboratory testing bench-top gravure printer from Schläfli-Maschinen. Finally, the source and drain contacts are deposited in the same manner as the gate electrodes.

Ink characterization: Contact angles were measured using a Krüss DSA100 contact angle goniometer and viscosities were obtained using a Cambridge Viscosity VISCOlab 4000 viscometer.

Surface characterization: Optical micrographs were obtained using a Zeiss Axioplan microscope and AFM measurements were performed using a Digital Instruments Dimension 3100 AFM in tapping mode.

Electrical characterization: Impedance measurements were performed using a Solartron Analytical 1260A impedance analyzer. The transistor characteristics were obtained in air using an Agilent 4156C semiconductor parameter analyzer.

Acknowledgements
This work has been supported by the European Commission's 7th Framework Programme (FP7/2007-2013) under grant agreement n° 607896 (OrgBIO).

Received:
Revised:
Published online:

References

[1] G. H. Gelinck, H. E. a Huitema, E. van Veenendaal, E. Cantatore, L. Schrijnemakers, J. B. P. H. van der Putten, T. C. T. Geuns, M. Beenhakkers, J. B. Giesbers, B.-H. Huisman, E. J. Meijer, E. M. Benito, F. J. Touwslager, A. W. Marsman, B. J. E. van Rens, D. M. de Leeuw, *Nat. Mater.* **2004**, *3*, 106.

[2] V. Subramanian, J. M. J. Fréchet, P. C. Chang, S. Member, D. C. Huang, J. B. Lee, S. Member, S. E. Molesa, S. Member, A. R. Murphy, D. R. Redinger, S. Member, S. K. Volkman, *Proc. IEEE* **2005**, *93*.

[3] L. Torsi, A. Dodabalapur, L. Sabbatini, P. G. Zambonin, *Sensors Actuators B Chem.* **2000**, *67*, 312.

[4] J. T. Mabeck, G. G. Malliaras, *Anal. Bioanal. Chem.* **2006**, *384*, 343.

[5] M. Berggren, A. Richter-Dahlfors, *Adv. Mater.* **2007**, *19*, 3201.

[6] J. Rivnay, R. M. Owens, G. G. Malliaras, *Chem. Mater.* **2014**, *26*, 679.

[7] E. Said, O. Larsson, M. Berggren, X. Crispin, *Adv. Funct. Mater.* **2008**, *18*, 3529.

[8] A. Facchetti, M.-H. Yoon, T. J. Marks, *Adv. Mater.* **2005**, *17*, 1705.

[9] M. J. Panzer, C. D. Frisbie, *Adv. Mater.* **2008**, *20*, 3176.

[10] L. Kergoat, B. Piro, M. Berggren, G. Horowitz, M. C. Pham, *Anal. Bioanal. Chem.* **2012**, *402*, 1813.

[11] G. Tarabella, F. M. Mohammadi, N. Coppede, F. Barbero, S. Iannotta, C. Santato, F. Cicoira, *Chem. Sci.* **2013**, *4*, 1395.

[12] D. Khodagholy, J. Rivnay, M. Sessolo, M. Gurfinkel, P. Leleux, L. H. Jimison, E. Stavrinidou, T. Herve, S. Sanaur, R. M. Owens, G. G. Malliaras, *Nat. Commun.* **2013**, *4*, 2133.

[13] Y. Xia, J. H. Cho, J. Lee, P. P. Ruden, C. D. Frisbie, *Adv. Mater.* **2009**, *21*, 2174.

[14] M. J. Panzer, C. R. Newman, C. D. Frisbie, *Appl. Phys. Lett.* **2005**, *86*, 103503.

[15] J. Lee, M. J. Panzer, Y. He, T. P. Lodge, C. D. Frisbie, *J. Am. Chem. Soc.* **2007**, *129*, 4532.

[16] E. Said, X. Crispin, L. Herlogsson, S. Elhag, N. D. Robinson, M. Berggren, *Appl. Phys. Lett.* **2006**, *89*, 143507.

[17] Y. Xia, W. Zhang, M. Ha, J. H. Cho, M. J. Renn, C. H. Kim, C. D. Frisbie, *Adv. Funct. Mater.* **2010**, *20*, 587.

[18] W. J. Hyun, E. B. Secor, G. A. Rojas, M. C. Hersam, L. F. Francis, C. D. Frisbie, *Adv. Mater.* **2015**, *27*, 7058.

[19] H. Sinno, H. T. Nguyen, A. Hägerström, M. Fahlman, L. Lindell, O. Coulembier, P. Dubois, X. Crispin, I. Engquist, M. Berggren, *Org. Electron. physics, Mater. Appl.* **2013**, *14*, 790.

[20] M. M. Voigt, A. Cuite, D. Y. Chung, R. U. A. Khan, A. J. Campbell, D. D. C. Bradley, F. Meng, J. H. G. Steinke, S. Tierney, L. McCulloch, H. Penxten, L. Luisen, O. Douheret, J. Manca, U. Brokmann, K. Sönnichsen, D. Hülsenberg, W. Bock, C. Barron, N. Blanckaert, S. Springer, J. Grupp, A. Mcsley, *Adv. Funct. Mater.* **2010**, *20*, 239.

[21] G. Grau, J. Cen, H. Kang, R. Kitsomboonloha, W. J. Scheideler, V. Subramanian, *Flex. Print. Electron.* **2016**, *1*, 1.

[22] N. L. Vaklev, Y. Yang, B. V. O. Muir, J. H. G. Steinke, A. J. Campbell, *IEEE Trans. Electron Devices* **2015**, *62*, 3820.

[23] A. C. Huebler, F. Doetz, H. Kempa, H. E. Katz, M. Bartzsch, N. Brandt, I. Hennig, U. Fuegmann, S. Vaidyanathan, J. Granstrom, S. Liu, A. Sydorenko, T. Zillger, G. Schmidt, K. Preissler, E. Reichmanis, P. Eckerle, F. Richter, T. Fischer, U. Hahn, *Org. Electron. physics, Mater. Appl.* **2007**, *8*, 480.

[24] M. Hambsch, K. Reuter, M. Stanel, G. Schmidt, H. Kempa, U. Fügmann, U. Hahn, A. C. Hübler, *Mater. Sci. Eng. B Solid-State Mater. Adv. Technol.* **2010**, *170*, 93.

[25] H. Kempa, M. Hambsch, K. Reuter, M. Stanel, G. C. Schmidt, B. Meier, A. C. Hübler, *IEEE Trans. Electron Devices* **2011**, *58*, 2765.

[26] N. L. Vaklev, R. Müller, B. V. O. Muir, D. T. James, R. Pretot, P. Van Der Schaaf, J. Genoe, J. S. Kim, J. H. G. Steinke, A. J. Campbell, *Adv. Mater. Interfaces* **2014**, *1*, 1.

[27] G. Grau, V. Subramanian, *Adv. Electron. Mater.* **2016**, *2*, 1500328.

[28] D. Tobjörk, N. J. Kaihovirta, T. Mäkelä, F. S. Pettersson, R. Österbacka, *Org. Electron. physics, Mater. Appl.* **2008**, *9*, 931.

[29] N. J. Kaihovirta, D. Tobjörk, T. Mäkelä, R. Österbacka, *Appl. Phys. Lett.* **2008**, *93*, 53302.

[30] H. G. O. Sandberg, T. G. Bäcklund, R. Österbacka, H. Stubb, *Adv. Mater.* **2004**, *16*, 1112.

[31] D. Y. Chung, J. Huang, D. D. C. Bradley, A. J. Campbell, *Org. Electron.* **2010**, *11*, 1088.

[32] S. Song, C. Peng, *J. Dispers. Sci. Technol.* **2008**, *29*, 1367.

[33] F. Machui, S. Langner, X. Zhu, S. Abbott, C. J. Brabec, *Sol. Energy Mater. Sol. Cells* **2012**, *100*, 138.

[34] R. J. Kline, M. D. McGehee, E. N. Kadnikova, J. Liu, J. M. J. Fréchet, *Adv. Mater.* **2003**, *15*, 1519.

[35] O. Larsson, E. Said, M. Berggren, X. Crispin, *Adv. Funct. Mater.* **2009**, *19*, 3334.

[36] M. J. Panzer, C. D. Frisbie, *Adv. Funct. Mater.* **2006**, *16*, 1051.

Figures

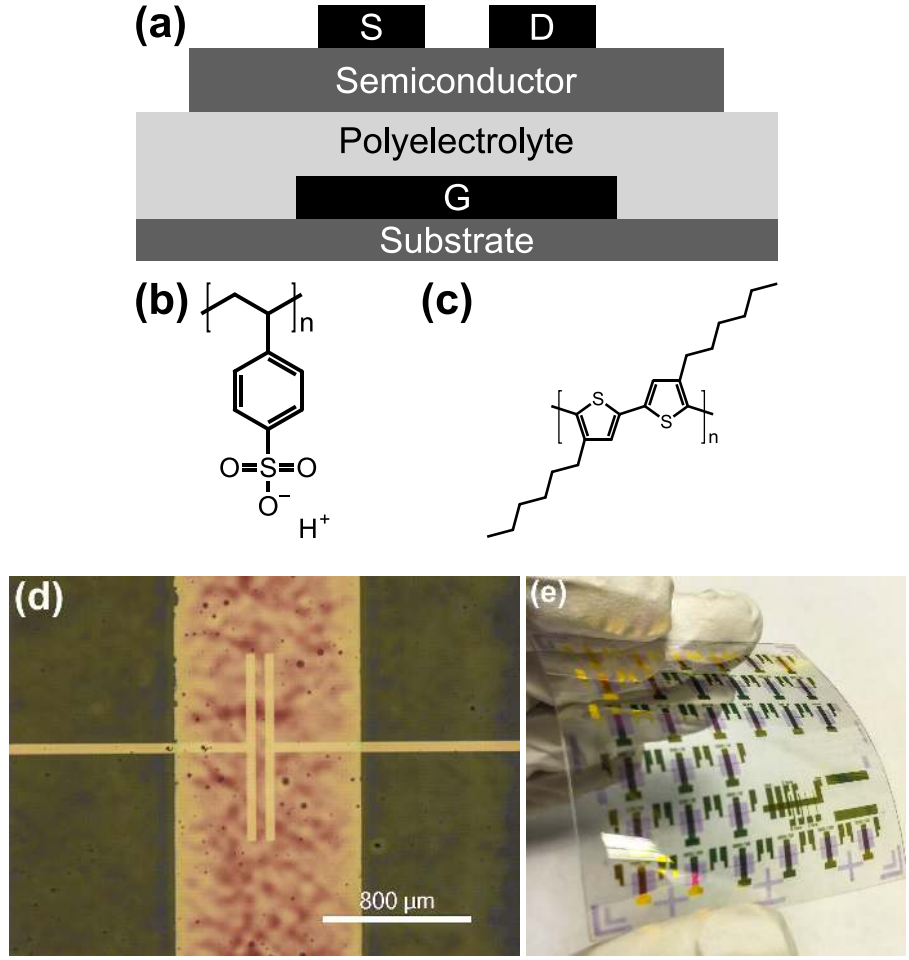

Figure 1. Schematic cross-section (a) of the device and chemical structure of the polyelectrolyte, PSSH, in its deprotonated state (b) and of the polymer semiconductor, regioregular P3HT (c). Optical micrograph (d) of a gravure-printed EGOFET. Photograph of an array of printed devices (e).

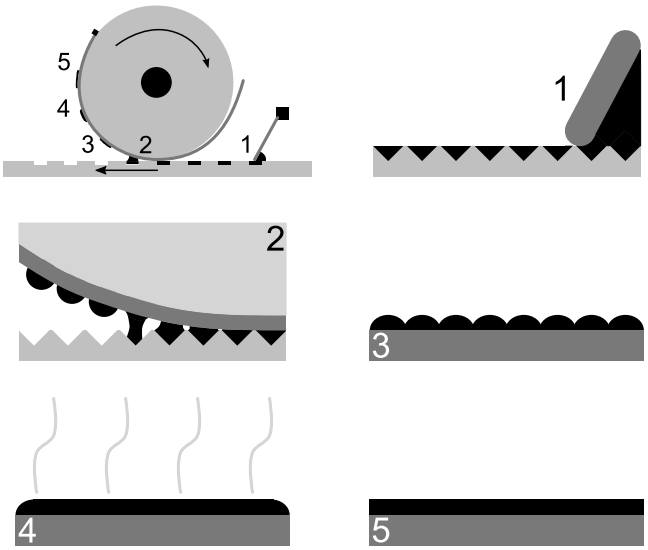

Figure 2. Schematics of the gravure printing process: the ink cells are filled via doctor blading of the cliché (1), the ink is transferred to the substrate by direct contact (2), the individual ink droplets spread and coalesce (3), the solvent evaporates (4) and a thin-film is obtained (5).

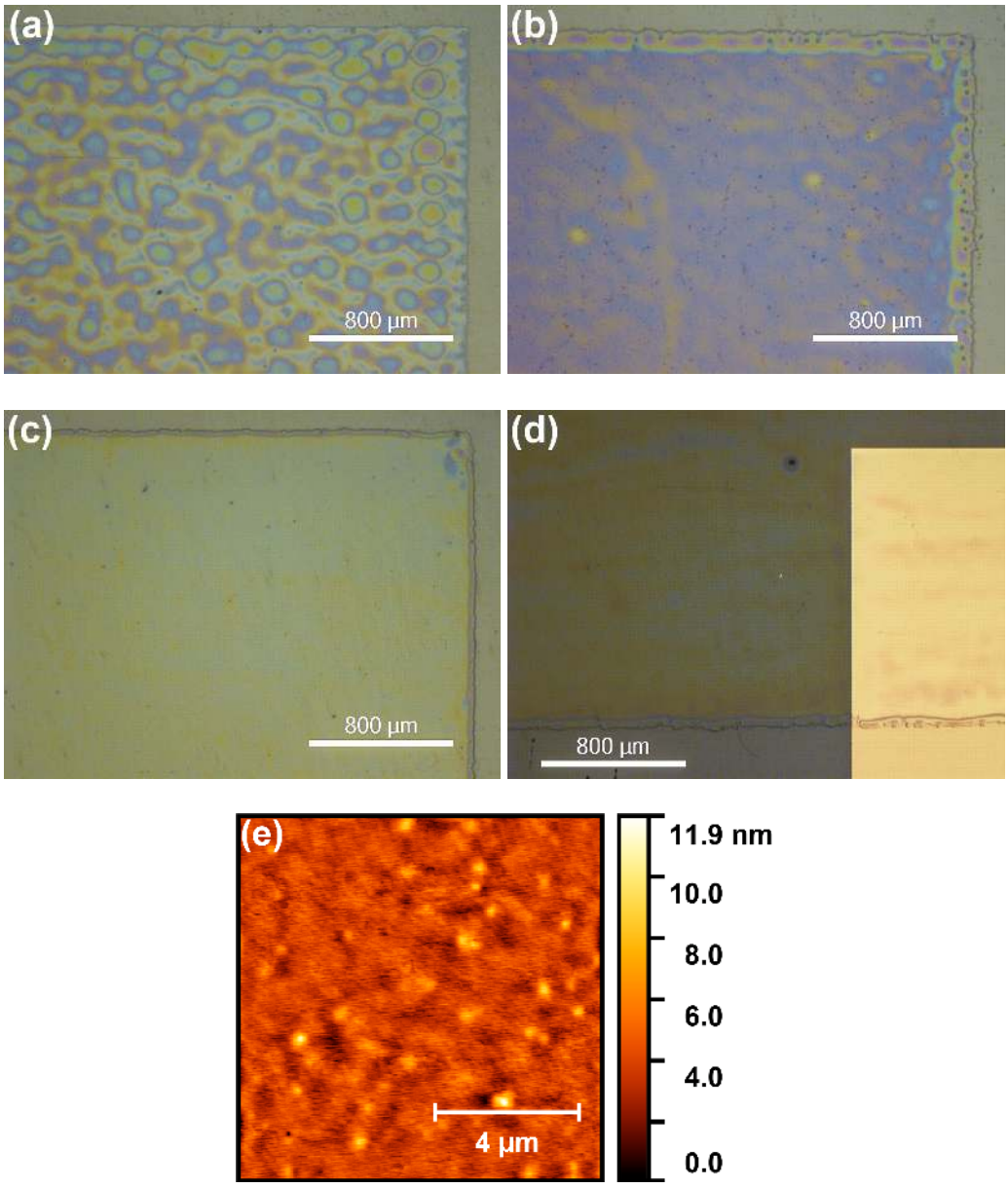

Figure 3. Optical micrographs (magnification x2.5) showing the edge of gravure printed PSSH films on PET substrates obtained from aqueous solutions (18 wt% in H_2O) with 0 vol% (a), 20 vol% (b) and 50 vol% (c) added isopropanol. The 50 vol% isopropanol formulation printed on top of a 50 nm-thick gold pad is also shown (d). AFM topography micrograph of the 50 vol% isopropanol formulation printed on PET (e).

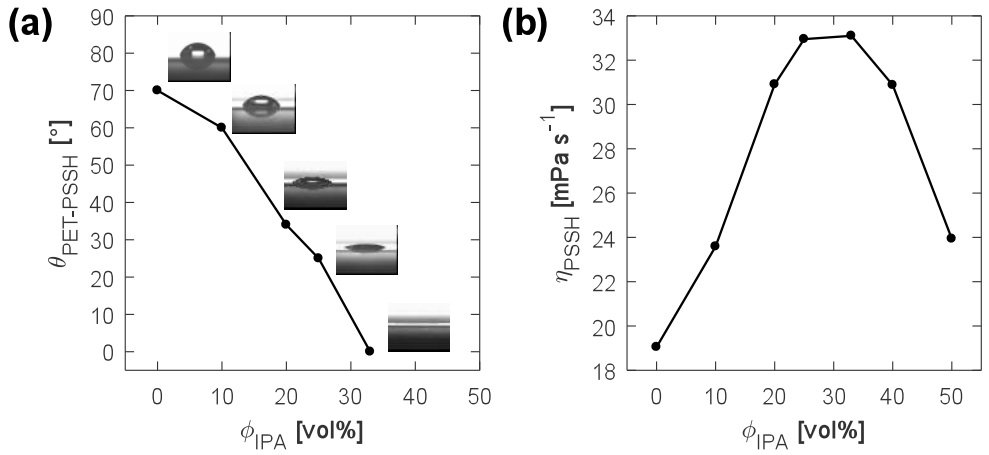

Figure 4. Contact angle $\theta_{PET\text{-}PSSH}$ on PET substrate (a) and viscosity η_{PSSH} (b) of PSSH aqueous solutions (18 wt% in H_2O) with various isopropanol volume fractions ϕ_{IPA}.

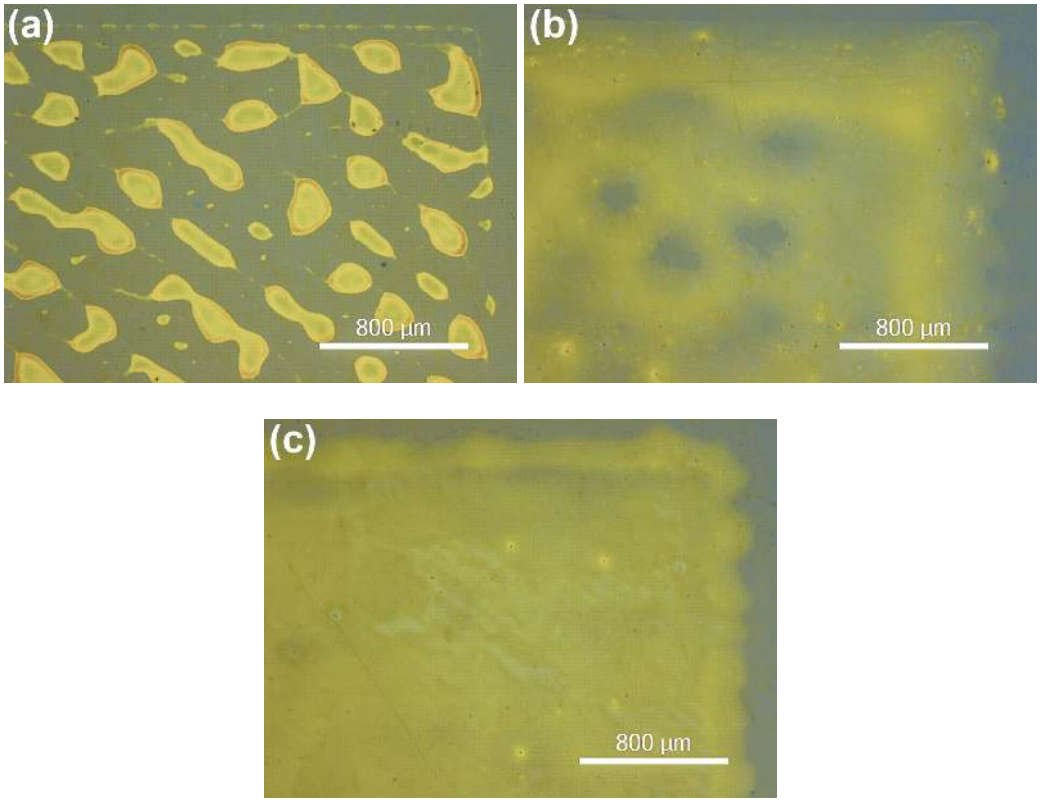

Figure 5. Optical micrographs (magnification x2.5) showing the edge of gravure printed P3HT films on PSSH, obtained from 10 mg mL^{-1} formulations in o-DCB (a), tetralin (b) and tetralin blended with cyclohexane in a 1:1 volume ratio (c).

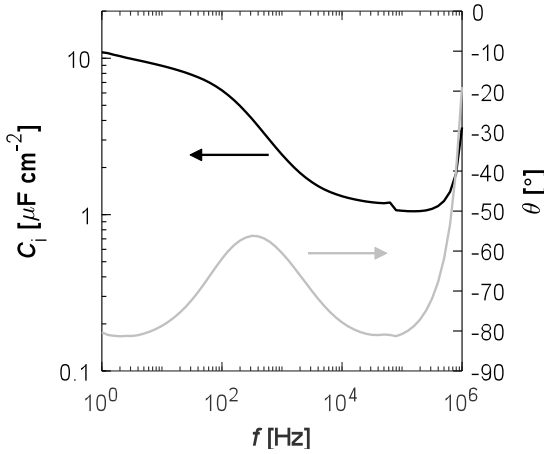

Figure 6. Frequency dependence of the effective capacitance per unit area C_i and phase angle θ of a gold/PSSH/gold capacitor.

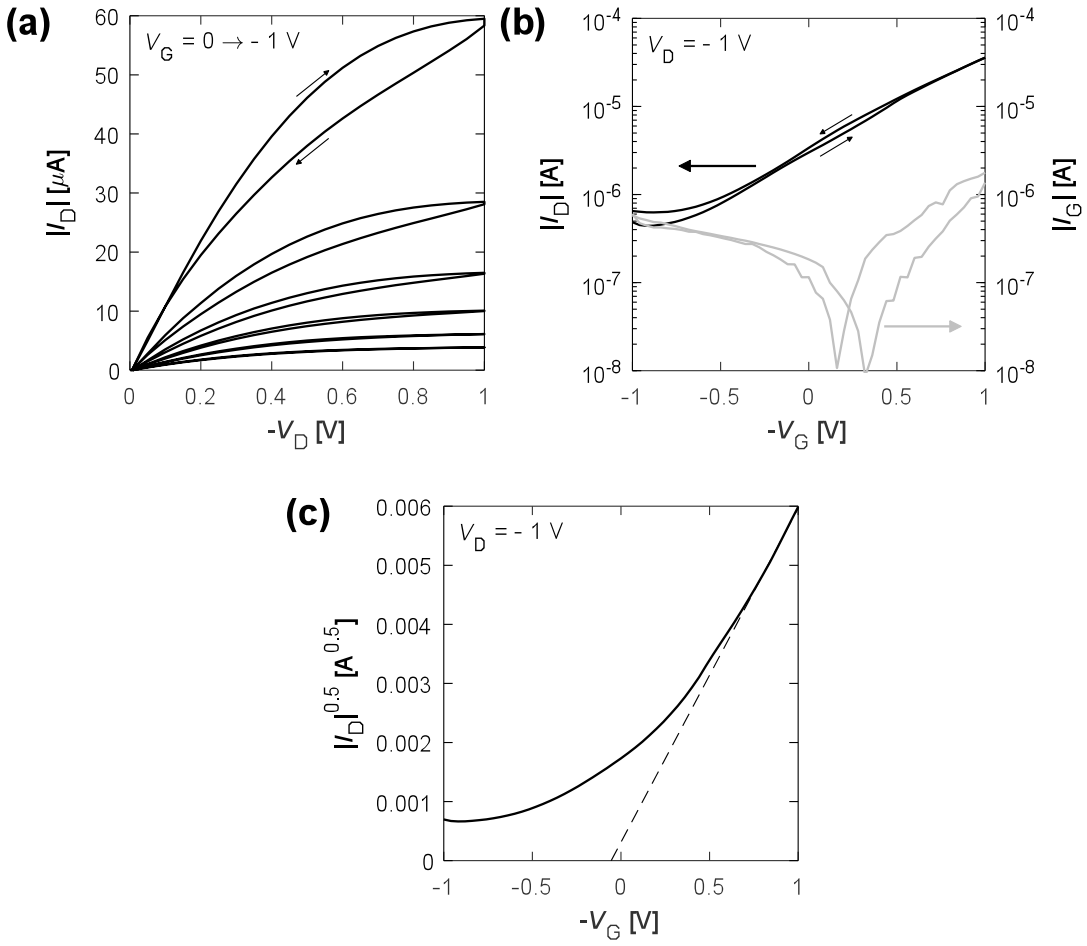

Figure 7. Characteristics obtained for a device with L = 20 μm: output characteristics (a), transfer characteristics with gate leakage current (b) and square root of the drain current versus the gate voltage for parameter extraction (the dashed line shows the extrapolated linear behavior) (c).